Terra Nova

Tomographic snapshot of an extinct, Late Mesoproterozoic mantle wedge beneath SW Fennoscandia

Journal:	*Terra Nova*
Manuscript ID	Draft
Wiley - Manuscript type:	Paper
Date Submitted by the Author:	n/a
Complete List of Authors:	Slagstad, Trond; Geological Survey of Norway, Maystrenko, Yuriy; Norges geologiske undersokelse Maupin, Valerie; Universitetet i Oslo Senter for Jordens utvikling og dynamikk Gradmann, Sofie; Norges geologiske undersokelse
Keywords:	tomography, Sveconorwegian, mantle wedge, Norway, Mesoproterozoic

Tomographic snapshot of an extinct, Late Mesoproterozoic mantle wedge beneath SW Fennoscandia

Trond Slagstad[1], Yuriy Maystrenko[1], Valerie Maupin[2], Sofie Gradmann[1]

[1]Geological Survey of Norway, PO Box 6315 Sluppen, 7491 Trondheim, Norway

[2]Centre for Earth Evolution and Dynamics, University of Oslo, PO Box 1028 Blindern, 0316 Oslo, Norway

Abstract

A channel-like, low-velocity zone in the lithospheric mantle beneath W Norway coincides spatially with the extension of a newly discovered 200 x 50 km granite batholith, which formed as a result of oceanic subduction beneath the SW Fennoscandian margin between 1.06 and 1.02 Ga. Based on results from numerical modeling, we argue that the low-velocity zone most likely represents the thermal (radioactive) and compositional (refertilized) effects of the mantle wedge of this magmatic arc. The geologic record in SW Fennoscandia suggests that active-margin magmatism terminated as a result of rapid slab roll-back and trench retreat starting at ca. 1 Ga. The rapid shift from active- to passive-margin processes was probably critical to preserve the mantle wedge, and their identification can therefore shed light on how active-margin processes terminated in ancient orogens.

Keywords: tomography, Sveconorwegian, mantle wedge, Norway, Mesoproterozoic

Introduction

Continental lithospheric mantle (CLM) typically displays a large range in seismic velocities, generally ascribed to recent or ongoing asthenospheric thermal events, variable melt depletion/refertilization, or juxtaposition of tectonic blocks with contrasting lithospheric structures. Metasomatism by asthenospheric upwellings and in mantle wedges above subducting oceanic slabs are the most likely candidates for refertilizing the CLM (Griffin et al., 2009). In general, however, it is difficult to attribute a particular anomaly in Archean/Proterozoic lithospheric mantle to specific geologic events or processes. Anomalously low seismic velocities can be confidently related to the thermal effects of mantle upwellings in regions of active intraplate magmatism (e.g., Civiero et al., 2015), while the effects of refertilization by ancient asthenospheric upwelling events may be inferred below some major magmatic centers, such as the ca. 2.05 Ga Bushveld Complex in South Africa (Fouch et al., 2004). Mantle wedges, however, are prone to destruction by continued active-margin processes, such as trench advance, opening of back-arc basins, and terminal continent-continent collision, resulting in a very low preservation potential. Localizing ancient, extinct mantle wedges requires that we recognize their seismic signature.

The ca. 1.1–0.9 Ga Sveconorwegian orogen in SW Fennoscandia was recently redefined from a Himalayan-type continent-continent collisional orogen to an accretionary orogen, with continuous subduction of oceanic crust along the SW Fennoscandian margin (Slagstad et al., 2013, 2017; Bybee et al., 2014; Coint et al., 2015). A large, 1.06–1.02 Ma granite batholith (the Sirdal Magmatic Belt, SMB) in SW Norway (Fig. 1A) is one of the key evidences for oceanic subduction, and appears to have been followed by rapid trench retreat, leaving behind a passive margin by 0.9 Ga. New geochronologic data (Wiest, 2016; Electronic Supplement

A) suggest a continuation of the SMB along the W Norwegian coast, coinciding spatially with a sharply defined, channel-like, low-velocity anomaly in the underlying lithospheric mantle (Fig. 1B; Kolstrup et al., 2015). Based on geologic/tectonic considerations and the results of numerical modeling to assess the thermal effects of enrichment in heat-producing elements (HPE; U, Th, K), we suggest that the channel-like mantle feature beneath W Norway most likely represents the thermal (radioactive) and compositional (refertilized) effects of a Sveconorwegian, ca. 1.0 Ga mantle wedge.

A Sveconorwegian active continental margin between 1.06 and 0.92 Ga

The SMB (Fig. 1A) is a recently discovered, major granite batholith that formed between 1.06 and 1.02 Ga, and interpreted to reflect the development of a long-lived continental-margin arc on the SW margin of Fennoscandia (Fig. 2; Slagstad et al., 2013, 2017; Coint et al., 2015). A sample of the Løvstakken granitic gneiss in Bergen (Fig. 1A) yields a concordia age of 1030 ± 8 Ma (MSWD = 1.08), interpreted as the crystallization age of the granite protolith (Electronic Supplement A), that, along with recent geochronologic data from the same region (Wiest, 2016), suggest a continuation of the SMB to the NNW along the W Norwegian coast. These new data suggest that the SMB is at least 300 km long, and extends along much of the west coast of Norway.

An apparent lull in magmatic activity between 1.02 and 0.99 Ga was followed by widespread granitic magmatism between 0.99 and 0.92 Ga (e.g., Vander Auwera et al., 2003). These younger granites have more ferroan compositions than the SMB and intruded throughout most of the orogen (Fig. 1A), and Slagstad et al. (2013, 2017) interpreted them to reflect continental back-arc extension during roll-back of the subducting oceanic lithosphere and

trench retreat. The geologic evidence from SW Fennoscandia therefore suggests that a period of oceanic subduction and continental-arc development was followed by trench retreat, ending in the inferred development of a passive continental margin, or a region far inboard of a still-active margin. Fig. 2A–C shows a schematic tectonic cartoon illustrating the Sveconorwegian orogenic evolution.

Low seismic-velocity channel beneath W Norway; recent or ancient?

Seismic tomographic data from SW Fennoscandia reveal a distinct channel-like, low-velocity zone in the lithospheric mantle and, to a lesser degree, in the underlying asthenosphere beneath W Norway (Fig. 1B; Kolstrup et al., 2015). Apart from a NE shift in direction in the northernmost part, the anomaly closely follows the inferred extent of the SMB (Fig. 1). Kolstrup et al. (2015) interpreted the channel-like feature to reflect a positive temperature anomaly, and proposed several potential heat sources, including (1) heating of the SW Fennoscandian CLM by influx of hot mantle material from the Iceland plume (e.g., Rickers et al., 2013), or (2) rifting related to opening of the North Atlantic at 55 Ma, or the late Paleo- to Mesozoic Oslo and Viking grabens (Fig. 1A). The identification of an extended SMB suggests a third possibility: (3) a refertilized, Sveconorwegian mantle wedge.

The thermal effects of three scenarios have been assessed through numerical modeling. Scenario 1 (mantle plume) models hot plume material impinging on the base of the lithosphere, raising the temperature at the lithosphere–asthenosphere boundary (LAB) by 100, 200, and 300°C above ambient temperature (1300°C). The model is time dependent and runs for 20 Myr, the maximum duration of Iceland-plume influence possible. Scenario 2 (rifting) models the effects of cooling following a rift event that increased the LAB temperature by 100, 200, and 300°C. The model is allowed to achieve steady-state conditions before LAB

95 temperatures are returned to ambient and the system is allowed to cool for 55 Myr. This
96 scenario models residual temperatures following a major heating event, such as rifting and
97 opening of the North Atlantic. Scenario 3 is a steady-state thermal model that shows the
98 effects of increased heat production in the mantle, mimicking a refertilized mantle wedge.
99 Heat production rates in the model wedge are 0.1, 0.2, and 0.5 $\mu W/m^3$ above ambient mantle
100 heat production (0.03 $\mu W/m^3$). The main model parameters and geometries for the different
101 scenarios are presented in Fig. 3A–C, the results are presented in Fig. 3D–F, and details
102 concerning the modeling are described in Electronic Appendix B.

103 The mantle temperature anomaly beneath Iceland is on the order of 100°C (Herzberg and
104 Gazel, 2009), but probably significantly lower 1000 km away from the hot spot, and the
105 plume appears to have been located in roughly its present position for ca. 20 Myr
106 (Thordarson, 2012). Barring the possibility of other sources of asthenosphere-derived material
107 than the Iceland plume, this provides a maximum temperature and duration for asthenosphere-
108 driven heating beneath SW Norway (scenario 1). Fig. 3D shows the time-dependent thermal
109 anomaly at 80 km depth related to hot asthenospheric material impinging on the base of 120
110 km-thick mantle lithosphere, corresponding roughly to the lithospheric thickness in SW
111 Norway (Maupin et al., 2013). Mantle material 100°C above ambient temperature results in a
112 maximum temperature anomaly around 25°C after 20 Myr, which is regarded as the
113 maximum possible thermal effect of the Iceland plume under SW Norway.

114 Opening of the North Atlantic at 55 Ma and late Paleo- to Mesozoic rifting in the Oslo and
115 Viking grabens (scenario 2), could have provided heat and refertilized the mantle lithosphere.
116 Our numerical modeling (Fig. 3E) shows that the thermal effects of such events decay to at
117 most a few tens of degrees after 55 Myr (ca. 15°C for 100°C anomaly). A temperature
118 perturbation of 300°C – much higher than even the most extreme mantle temperature
119 anomalies associated with large igneous provinces and ocean islands (Rooney et al., 2012) –

120 results in a present-day anomaly of ca. 40°C. Also, if Paleo- to Mesozoic rifting had
121 refertilized the CLM, we would expect to see these effects concentrated beneath the areas of
122 rifting. The low-velocity channel beneath W Norway is, however, not spatially associated
123 with any post-Sveconorwegian, rift-related magmatism.

124 The extent to which mantle wedges are enriched in HPE during oceanic subduction is difficult
125 to quantify. Earlier models of subduction-zone magmatism have focused on dehydration of
126 the oceanic slab and migration of the hydrous fluids into the mantle wedge, where they would
127 trigger melting (Kushiro, 1973). More recent work, however, suggests that temperatures in the
128 subduction channel may be high enough to allow water-fluxed partial melting of both the
129 downgoing slab and overlying sediments (Spandler and Pirard, 2013). The sediment-derived
130 melts, in particular, have a large potential for refertilizing the overlying mantle wedge and
131 lower arc crust (Hacker et al., 2011). In addition, partial melts from eclogitized subducted
132 basalt may convert peridotite to olivine-free pyroxenite (Sobolev et al., 2007), which is
133 characterized by higher concentrations of HPE than peridotite (Rybach and Čermak, 1982). A
134 realistic estimate may be around 0.1 $\mu W/m^3$ for metasomatized lithosphere (Rudnick et al.,
135 1998), but as shown by these authors, mantle xenoliths display variation of 2–3 orders of
136 magnitude. The steady-state thermal anomaly associated with a realistic value of 0.1 $\mu W/m^3$
137 is ca. 40°C (Fig. 3F) at 60 km depth. This anomaly is similar to the maximum, and possibly
138 unrealistically high, model anomalies expected from younger thermal events. Higher values of
139 0.3 to 0.4 $\mu W/m^3$ produce temperature anomalies of 100 to 150°C.

140 Subduction beneath SW Fennoscandia between 1.06 and 1.020 Ga may have rehydrated and
141 refertilized the mantle wedge, including adding HPE. Our numerical modeling shows that
142 variations in HPE can result in long-lived (governed by radioactive decay rates) temperature
143 anomalies on the order of several tens of degrees. A long-extinct mantle wedge would,

144 therefore, be expected to be hotter than ambient lithospheric mantle, as well as more hydrous
145 and fertile, and to show up in tomographic models as a well-defined low-velocity channel.

146 Temperature is recognized as the major parameter affecting lithospheric seismic velocities,
147 and their relationship depends on several, poorly constrained factors, in particular grain size
148 (Cammarano et al., 2003; Faul and Jackson, 2005). Body-wave tomography, as in Kolstrup et
149 al. (2015), provides information on the relative variations in seismic velocities, but not their
150 absolute values, increasing the uncertainty between velocity and temperature (Cammarano et
151 al., 2003). Kolstrup et al. (2015) discuss this issue and argue for a ca. 350°C difference
152 between the cold, Swedish lithosphere and the channel in western Norway. Compared to the
153 warmer lithosphere in southern Norway, we estimate that a temperature anomaly of 150–
154 200°C would explain the low seismic-velocity channel. Although the most realistic heat-
155 production values for a mantle wedge fails to produce such high temperatures, it comes closer
156 that the other hypothesized scenarios. Fertile compositions are also likely to reduce seismic
157 velocities (Gradmann et al., 2013), and in addition, metasomatized mantle would be prone to
158 low degrees of phlogopite-dehydration melting given an increase in temperature (cf., Finn et
159 al., 2005), which would reduce seismic velocities significantly. This process is, however,
160 difficult to prove in the magmatically quiescent SW Fennoscandia.

161 The suggestion that the low-velocity, channel-like feature under W Norway represents an
162 extinct, Sveconorwegian mantle wedge does not rule out influx of asthenospheric mantle
163 material from the Iceland plume. The two processes may have acted in concert, with the
164 mantle wedge determining the geometry of the feature and asthenospherically derived heat
165 enhancing it. This interplay is similar to that proposed for E Australia, where influx of hot
166 Pacific asthenosphere triggers melting in a Cretaceous mantle wedge resulting in alkaline
167 magmatism (Finn et al., 2005).

Tectonic significance of preserved mantle wedges

The Sveconorwegian orogeny marked the end of >800 Myr of active-margin processes on the SW margin of Fennoscandia (Roberts and Slagstad, 2015), yet to our knowledge, the Fennoscadian CLM does not contain similar anomalies that can easily be interpreted as extinct mantle wedges. This observation suggests that mantle wedges, which represent sites of extensive CLM refertilization, have a very low preservation potential and require a certain sequence of events to be preserved in the geologic record.

In the Sveconorwegian case, rapid slab roll-back and trench retreat took place sometime between 0.99 and 0.92 Ga, leaving behind a passive margin (Slagstad et al., 2013, 2017). We suggest that this rapid roll-back may have aided preservation of the mantle wedge. A similar, younger example comes from E Australia, where an extinct mantle wedge appears to be the locus of Cenozoic alkaline magmatism (Finn et al., 2005). As suggested for the much older Sveconorwegian case, the tectonic regime along eastern Australia changed from long-lived subduction until ca. 110 Ma, followed by crustal extension and eastward drift of Zealandia starting at ca. 105 Ma (Bradshaw, 1989), leaving behind a passive continental margin underlain by an extinct mantle wedge.

A rapid change from active- to passive-margin tectonics, without an intervening collision, is clearly favorable for preserving mantle wedges in the CLM. In contrast, the mantle wedge related to subduction of Tethyan oceanic lithosphere under Asia (e.g., Zhang et al., 2013), prior to the onset of India–Asia collision at ca. 70 Ma (Yin and Harrison, 2000), is unlikely to be preserved for posterity due to the ongoing collision which is probably in the processes of eradicating all evidence of the pre-collisional processes from the Asian CLM (e.g., Molnar et al., 1993).

Conclusions

The formation and preservation of a ca. 1 Ga Sveconorwegian mantle wedge under W Norway is consistent with geologic evidence, and can explain a well-defined, low-velocity channel beneath SW Fennoscandia. We suggest that the low seismic velocities are the combined result of anomalously high temperatures due to radiogenic heating and enriched mantle compositions, both a result of refertilization during arc magmatism. Rapid trench retreat with formation of a passive margin, far inboard of a potentially still-active continental margin, appears to be a critical factor in mantle-wedge preservation. Metasomatized CLM in subduction zones that terminate in continent-continent collisions are unlikely to be preserved. Preservation of metasomatized CLM probably requires a special sequence of tectonic events, and their identification may, therefore, provide additional information on ancient, orogenic processes.

Acknowledgements

We wish to thank Torkil Røhr and Øyvind Skår for help with the dating of the Løvstakken granite, within the auspices of the COOP-project (#362200). Bill Griffin, Jörg Ebbing, and an anonymous reviewer provided helpful comments to an earlier version of the paper.

References cited

Bradshaw, J.D., 1989. Cretaceous geotectonic patterns in the New Zealand Region *Tectonics*, **8**, 803-820.

Bybee, G.M., Ashwal, L.D., Shirey, S.B., Horan, M., Mock, T. and Andersen, T.B., 2014. Pyroxene megacrysts in Proterozoic anorthosites: Implications for tectonic setting, magma source and magmatic processes at the Moho *Earth and Planetary Science Letters*, **389**, 74-85.

Cammarano, F., Goes, S., Vacher, P. and Giardini, D., 2003. Inferring upper-mantle temperatures from seismic velocities *Physics of the Earth and Planetary Interiors*, **138**, 197-222.

Civiero, C., Hammond, J.O.S., Goes, S., Fishwick, S., Ahmed, A., Ayele, A., Doubre, C., Goitom, B., Keir, D., Kendall, J.M., Leroy, S., Ogubazghi, G., Rümpker, G. and

Stuart, G.W., 2015. Multiple mantle upwellings in the transition zone beneath the northern East-African Rift system from relative P-wave travel-time tomography *Geochemistry, Geophysics, Geosystems*, **16**, 2949-2968.

Coint, N., Slagstad, T., Roberts, N.M.W., Marker, M., Røhr, T. and Sørensen, B.E., 2015. The Late Mesoproterozoic Sirdal Magmatic Belt, SW Norway: Relationships between magmatism and metamorphism and implications for Sveconorwegian orogenesis *Precambrian Research*, **265**, 57-77.

Faul, U.H. and Jackson, I., 2005. The seismological signature of temperature and grain size variations in the upper mantle *Earth and Planetary Science Letters*, **234**, 119-134.

Finn, C.A., Müller, R.D. and Panter, K.S., 2005. A Cenozoic diffuse alkaline magmatic province (DAMP) in the southwest Pacific without rift or plume origin *Geochemistry, Geophysics, Geosystems*, **6**, n/a-n/a.

Fouch, M.J., James, D.E., VanDecar, J.C., van der Lee, S. and Group, K.S., 2004. Mantle seismic structure beneath the Kaapvaal and Zimbabwe Cratons *South African Journal of Geology*, **107**, 33-44.

Gradmann, S., Ebbing, J. and Fullea, J., 2013. Integrated geophysical modelling of a lateral transition zone in the lithospheric mantle under Norway and Sweden *Geophysical Journal International*, **194**, 1358-1373.

Griffin, W.L., O'Reilly, S.Y., Afonso, J.C. and Begg, G.C., 2009. The composition and evolution of lithospheric mantle: a re-evaluation and its tectonic implications *Journal of Petrology*, **50**, 1185-1204.

Hacker, B.R., Kelemen, P.B. and Behn, M.D., 2011. Differentiation of the continental crust by relamination *Earth and Planetary Science Letters*, **307**, 501-516.

Herzberg, C. and Gazel, E., 2009. Petrological evidence for secular cooling in mantle plumes *Nature*, **458**, 619-622.

Kolstrup, M.L., Hung, S.-H. and Maupin, V., 2015. Multiscale, finite-frequency P and S tomography of the upper mantle in the southwestern Fennoscandian Shield *Geophysical Journal International*, **202**, 190-218.

Kushiro, I., 1973. Origin of some magmas in oceanic and circum-oceanic regions *Tectonophysics*, **17**, 211-222.

Maupin, V., Agostini, A., Artemieva, I., Balling, N., Beekman, F., Ebbing, J., England, R.W., Frassetto, A., Gradmann, S., Jacobsen, B.H., Köhler, A., Kvarven, T., Medhus, A.B., Mjelde, R., Ritter, J., Sokoutis, D., Stratford, W., Thybo, H., Wawerzinek, B. and Weidle, C., 2013. The deep structure of the Scandes and its relation to tectonic history and present-day topography *Tectonophysics*, **602**, 15-37.

Molnar, P., England, P.C. and Martinod, J., 1993. Mantle dynamics, uplift of the Tibetan plateau, and the Indian monsoon *Reviews of Geophysics*, **31**, 357-396.

Rickers, F., Fichtner, A. and Trampert, J., 2013. The Iceland–Jan Mayen plume system and its impact on mantle dynamics in the North Atlantic region: Evidence from full-waveform inversion *Earth and Planetary Science Letters*, **367**, 39-51.

Roberts, N.M.W. and Slagstad, T., 2015. Continental growth and reworking on the edge of the Columbia and Rodinia supercontinents; 1.86–0.9 Ga accretionary orogeny in southwest Fennoscandia *International Geology Review*, **57**, 1582-1606.

Rooney, T.O., Herzberg, C. and Bastow, I.D., 2012. Elevated mantle temperature beneath East Africa *Geology*, **40**, 27-30.

Rudnick, R.L., McDonough, W.F. and O'Connell, R.J., 1998. Thermal structure, thickness and composition of continental lithosphere *Chemical Geology*, **145**, 395-411.

Rybach, L. and Čermak, V., 1982. Thermal properties: Radioactive heat generation in rocks. In: *Physical Properties of Rocks* (G. Angenheister, ed, pp. 353-371. Springer, Berlin.

Slagstad, T., Roberts, N.M.W. and Kulakov, E., 2017. Linking orogenesis across a supercontinent; the Grenvillian and Sveconorwegian margins on Rodinia *Gondwana Research*, **44**, 109-115.

Slagstad, T., Roberts, N.M.W., Marker, M., Røhr, T.S. and Schiellerup, H., 2013. A non-collisional, accretionary Sveconorwegian orogen *Terra Nova*, **25**, 30-37.

Sobolev, A.V., Hofmann, A.W., Kuzmin, D.V., Yaxley, G.M., Arndt, N.T., Chung, S.-L., Danyushevsky, L.V., Elliott, T., Frey, F.A., Garcia, M.O., Gurenko, A.A., Kamenetsky, V.S., Kerr, A.C., Krivolutskaya, N.A., Matvienkov, V.V., Nikogosian, I.K., Rocholl, A., Sigurdsson, I.A., Sushchevskaya, N.M. and Teklay, M., 2007. The Amount of Recycled Crust in Sources of Mantle-Derived Melts *Science*.

Spandler, C. and Pirard, C., 2013. Element recycling from subducting slabs to arc crust: A review *Lithos*, **170–171**, 208-223.

Thordarson, T., 2012. Outline of Geology of Iceland. In: *AGU Chapman Conference on Volcanism and the Atmosphere*. AGU, Selfoss, Iceland.

Vander Auwera, J., Bogaerts, M., Liégeois, J.-P., Demaiffe, D., Wilmart, E., Bolle, O. and Duchesne, J.-C., 2003. Derivation of the 1.0.0.9 Ga ferro-potassic A-type granitoids of southern Norway by extreme differentiation from basic magmas *Precambrian Research*, **124**, 107-148.

Wiest, J., 2016. Mesoproterozoic to Early Devonian Evolution of the Lyderhorn Gneiss (Øygarden Complex, SW Norway). MSc, University of Bergen, Bergen, 128 p.

Yin, A. and Harrison, T.M., 2000. Geologic evolution of the Himalayan-Tibetan Orogen *Annual Review of Earth and Planetary Sciences*, **28**, 211-280.

Zhang, Z., Dong, X., Xiang, H., Liou, J.G. and Santosh, M., 2013. Building of the Deep Gangdese Arc, South Tibet: Paleocene Plutonism and Granulite-Facies Metamorphism *Journal of Petrology*, **54**, 2547-2580.

Captions

Fig. 1. (A) Simplified geologic map of the western and central Sveconorwegian Province, indicating the main magmatic features on which the tectonic model is based. The orange star

299 shows the location of the Løvstakken granite; a possible extension of the Sirdal Magmatic
300 Belt. (B) P-wave velocity anomalies at 100 km depth in the mantle lithosphere beneath SW
301 Fennoscandia, from Kolstrup et al. (2015), with the trace of the proposed Sveconorwegian
302 arc. The thick, dotted line indicates the trace of known Sveconorwegian arc magmatism.

303 Fig. 2. Cartoon illustrating the tectonic evolution of the Sveconorwegian orogen, based on
304 Slagstad et al. (2013, 2017).

305 Fig. 3. (A–C) Model geometries and parameters used for thermal modeling. See Electronic
306 Supplement B for additional details. (D) Time-dependent temperature anomaly at 80 km
307 depth in the mantle lithosphere as a result of variable heating (100–300°C above ambient
308 temperature) at the base of the lithosphere at 120 km depth. The model approximates the
309 effect of an external heat source, e.g., hot mantle material (plume), impinging on the base of
310 the lithosphere. (E) Time-dependent temperature decay at 80 km depth following a steady-
311 state situation with variable degrees of heating (100–300°C above ambient temperature) at the
312 base of the lithosphere at 120 km depth. The model approximates the effect of cooling after
313 long-lived heating, e.g., related to rifting. (F) Steady-state temperature anomaly resulting from
314 anomalous mantle, enriched in heat-producing elements, with heat-production rates between
315 0.1 and 0.5 $\mu W/m^3$ above ambient mantle heat production.

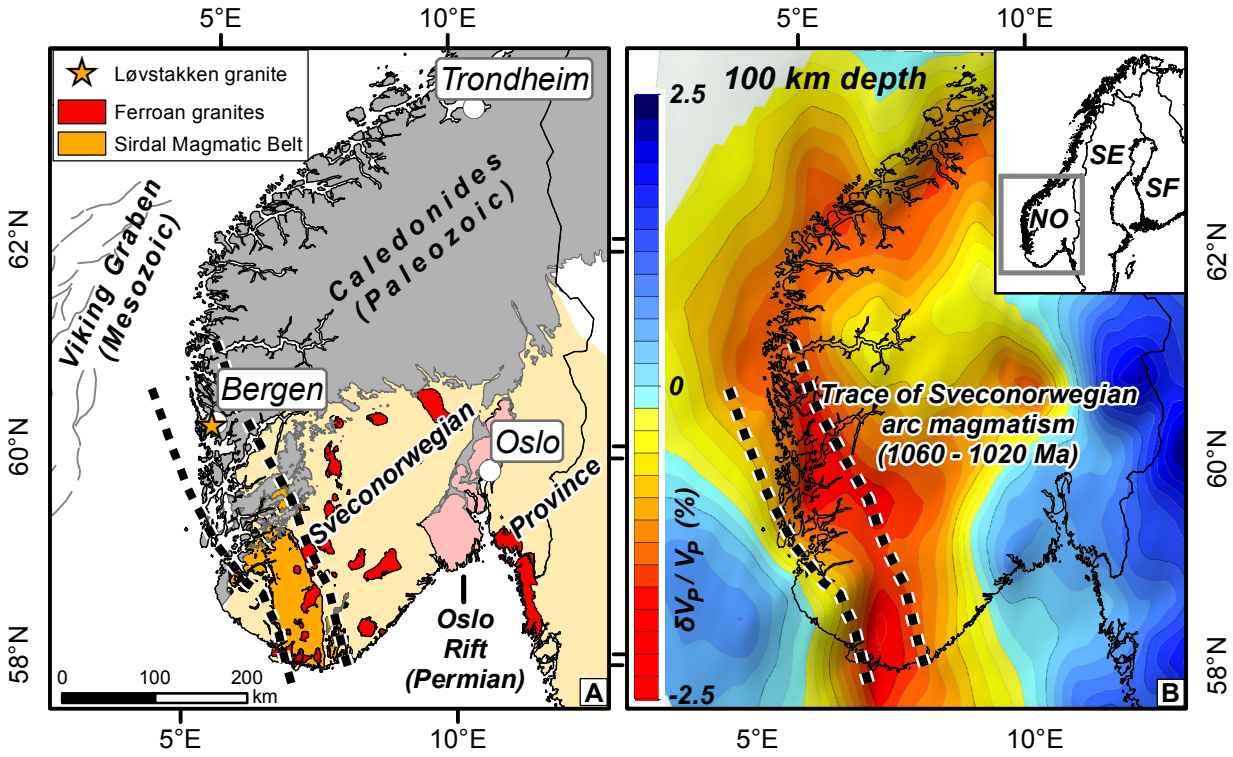
5°E
10°E
62°N
60°N
58°N
Løvstakken granite
Ferroan granites
Sirdal Magmatic Belt
Trondheim
Caledonides (Paleozoic)
Viking Graben (Mesozoic)
Bergen
Oslo
Sveconorwegian
Province
Oslo Rift (Permian)
0 100 200 km
A
100 km depth
2.5
0
-2.5
δVP / VP (%)
Trace of Sveconorwegian arc magmatism (1060 - 1020 Ma)
SE
SF
NO
B

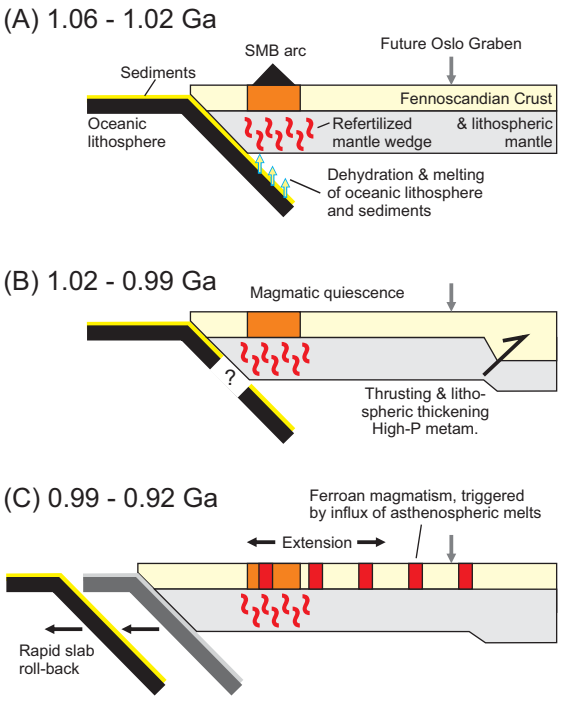
(A) 1.06 - 1.02 Ga
SMB arc
Future Oslo Graben
Sediments
Fennoscandian Crust
Oceanic lithosphere
Refertilized mantle wedge
& lithospheric mantle
Dehydration & melting of oceanic lithosphere and sediments
(B) 1.02 - 0.99 Ga
Magmatic quiescence
?
Thrusting & litho-spheric thickening High-P metam.
(C) 0.99 - 0.92 Ga
Ferroan magmatism, triggered by influx of asthenospheric melts
Extension
Rapid slab roll-back

(A) Scenario 1, mantle plume impinging on LAB. Heating over 20 Myr

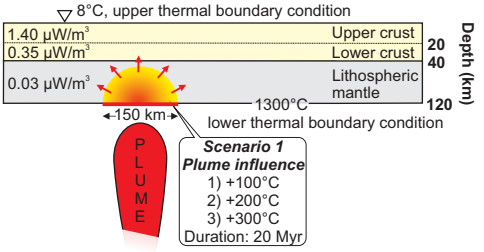

(B) Scenario 2, cooling for 55 Myr following rifting

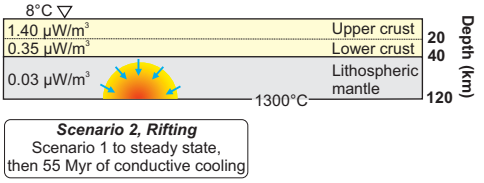

(C) Scenario 3, radioactively enriched mantle wedge

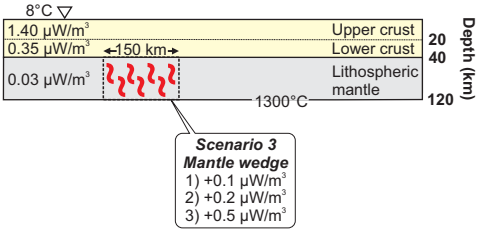

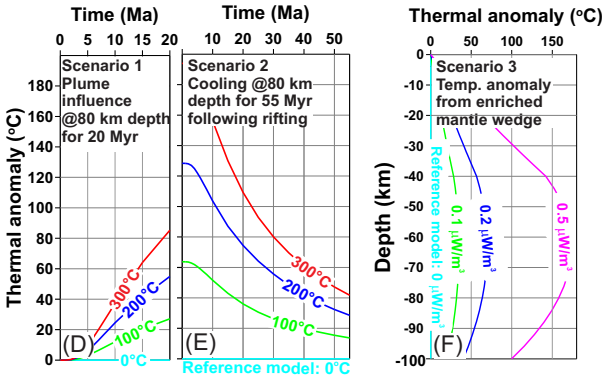

ELECTRONIC SUPPLEMENT A: U–Pb ZIRCON GEOCHRONOLOGY

METHOD

LA–ICP–MS (Laser Ablation Inductively Coupled Mass Spectrometry) analyses were carried out at the Geological Survey of Norway (NGU) on an ELEMENT XR single-collector, high-resolution ICP–MS, coupled to a UP193–FX 193 nm short-pulse excimer laser ablation system from New Wave Research. The laser was set to ablate single, up to 60 μm-long lines, using a spot size of 15 μm, a repetition rate of 10 Hz and an energy corresponding to a fluence of 4–5 J/cm^2. Each analysis included 30 s of background measurement followed by 30 s of ablation. The masses 202, 204, 206–208, 232 and 238 were measured. The reference material GJ–1 (Jackson et al., 2004) was used for correction of isotopic ratios, whereas 91500 (Wiedenbeck et al., 1995) and an in-house standard (OS–99–14; 1797 ± 3 Ma; Skår, 2002) were used to check precision and accuracy. The data were not corrected for common lead, but monitoring of the signal for 204 allowed exclusion of affected data from further calculations. The data were reduced using the GLITTER® software (Van Achterbergh et al., 2001).

U–PB ZIRCON DATA

The zircons from sample 064814, Løvstakken granite, (long/lat: 5.2789E/60.3419N) are prismatic, 100–200 μm, with CL-light, oscillatory-zoned cores rimmed by CL-dark, faintly oscillatory-zoned mantles that locally truncate the zoning of the cores (Fig. A1). The analytical data are presented in Table A1. Three analyses targeted CL-dark grains, but yielded strongly discordant or reversely discordant data. Nine analyses yield concordant data with a Concordia age of 1030 ± 8 Ma (MSWD = 1.08, Fig. A2). This age is interpreted to represent the crystallization age of the Løvstakken granite.

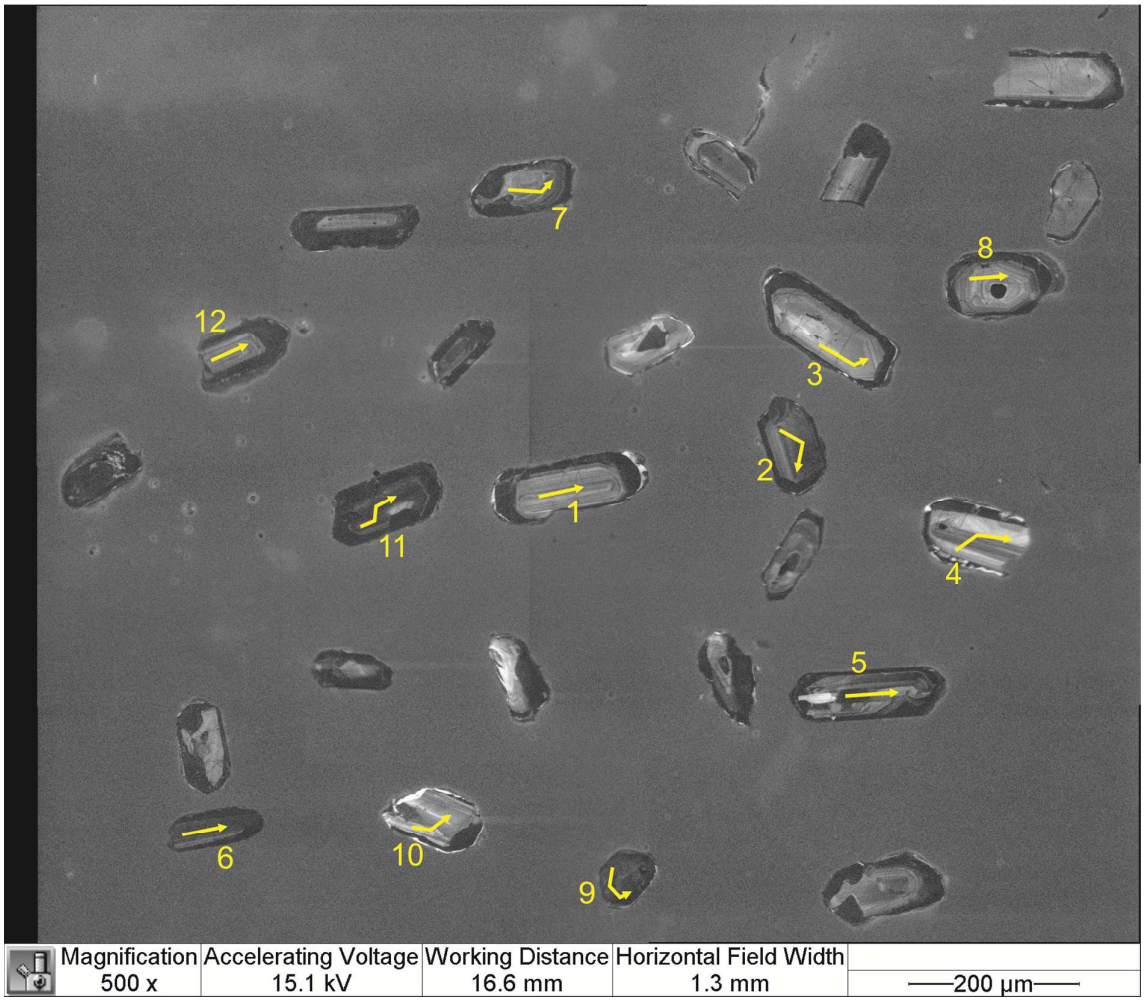

Fig. A1. CL images of zircons from sample 064814, Løvstakken granite, with arrows indicating were ablation lines for U–Pb isotopic analysis were made. The numbers correspond to the Analysis_# in Table A1.

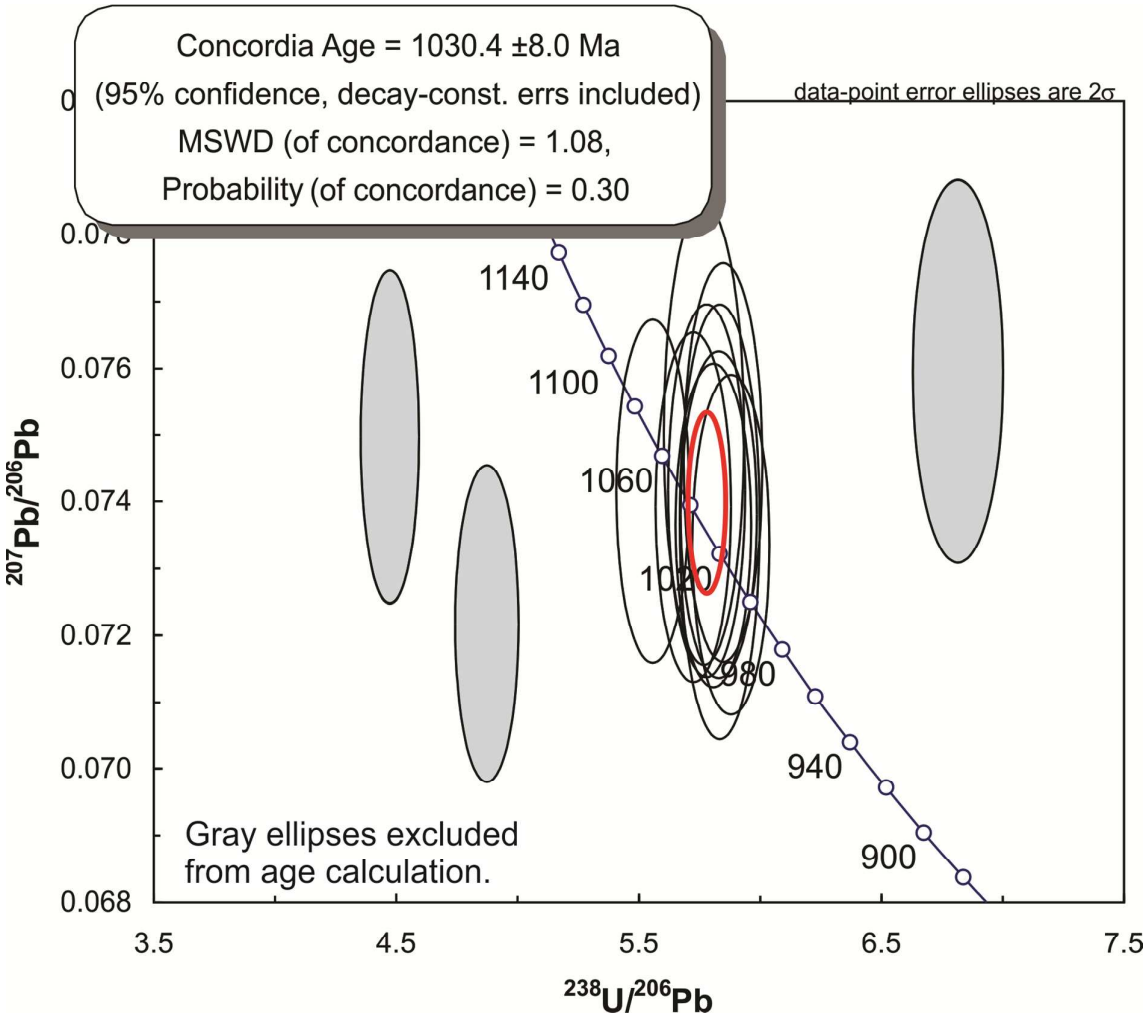

Fig. A2. Tera–Wasserburg diagram presenting the U–Pb zircon isotopic data from sample 064814. The gray ellipses have been excluded from the Concordia age calculation.

Table A1. Zircon U–Pb isotopic data from the Løvstakken granite, sample# 064814.

	Isotope ratios.									Age estimates (ma).							Concentrations				
	Concordia output					Terra-Wasserburg output															
Analysis_#	Pb207/U235	1s%	Pb206/U238	1s%	roh	238/206	1s%	207/206	1s%	Pb207/Pb206	1s	Pb207/U235	1s	Pb206/U238	1s	conc	U/Th	U	Th	Pbtot	Comments
LG064814_01	1.7931	1.89	0.17337	1.17	0.32	5.7680	1.17	0.07501	1.88	1068.6	37.3	1042.9	12.31	1030.6	11.16	96.4	0.9	197	176	39	
LG064814_02	1.7460	1.40	0.17154	1.10	0.43	5.8295	1.10	0.07381	1.35	1036.3	27.19	1025.7	9.04	1020.6	10.41	98.5	0.8	464	373	107	
LG064814_03	1.7422	1.81	0.17144	1.15	0.33	5.8329	1.15	0.07370	1.80	1033.2	35.98	1024.3	11.71	1020	10.92	98.7	0.8	151	118	34	
LG064814_04	1.7591	1.66	0.17103	1.13	0.36	5.8469	1.13	0.07459	1.64	1057.1	32.85	1030.5	10.72	1017.8	10.68	96.3	0.4	220	77	44	
LG064814_05	1.7807	1.49	0.17469	1.11	0.41	5.7244	1.11	0.07392	1.45	1039.3	29.08	1038.4	9.66	1037.9	10.65	99.9	0.5	333	170	82	
~~LG064814_06~~	~~2.3109~~	~~1.40~~	~~0.22354~~	~~1.10~~	~~0.43~~	~~4.4735~~	~~1.10~~	~~0.07497~~	~~1.36~~	~~1067.6~~	~~27.21~~	~~1215.6~~	~~9.94~~	~~1300.6~~	~~12.95~~	~~121.8~~	~~1.0~~	~~473~~	~~494~~	~~153~~	~~strongly reversely discordant~~
LG064814_07	1.7490	1.38	0.17221	1.10	0.43	5.8069	1.10	0.07365	1.34	1031.9	26.7	1026.8	8.95	1024.3	10.40	99.3	1.3	267	348	52	
LG064814_08	1.7698	1.56	0.17303	1.12	0.38	5.7793	1.12	0.07417	1.54	1046.1	30.7	1034.4	10.13	1028.8	10.65	98.3	0.6	204	130	42	
~~LG064814_09~~	~~2.0421~~	~~1.38~~	~~0.2052~~	~~1.10~~	~~0.43~~	~~4.8733~~	~~1.10~~	~~0.07217~~	~~1.34~~	~~990.7~~	~~27.05~~	~~1129.7~~	~~9.40~~	~~1203.2~~	~~12.04~~	~~121.4~~	~~0.2~~	~~560~~	~~95~~	~~175~~	~~strongly reversely discordant~~
LG064814_10	1.7207	1.44	0.17009	1.11	0.41	5.8792	1.11	0.07336	1.42	1024	28.32	1016.3	9.27	1012.6	10.34	98.9	0.7	210	144	41	
LG064814_11	1.8403	1.45	0.17996	1.11	0.41	5.5568	1.11	0.07416	1.42	1045.9	28.38	1060	9.54	1066.7	10.86	102.0	0.9	376	336	104	
~~LG064814_12~~	~~1.5366~~	~~1.56~~	~~0.14673~~	~~1.12~~	~~0.38~~	~~6.8152~~	~~1.12~~	~~0.07595~~	~~1.54~~	~~1093.6~~	~~30.53~~	~~945.1~~	~~9.60~~	~~882.6~~	~~9.22~~	~~80.7~~	~~0.5~~	~~292~~	~~156~~	~~56~~	~~strongly discordant~~

REFERENCES

Jackson, S. E., Pearson, N. J., Griffin, W. L., and Belousova, E. A., 2004, The application of laser ablation-inductively coupled plasma-mass spectrometry to in situ U-Pb zircon geochronology: Chemical Geology, v. 211, p. 47-69.

Skår, Ø., 2002, U-Pb geochronology and geochemistry of early Proterozoic rocks of the tectonic basement windows in central Nordland, Caledonides of north-central Norway: Precambrian Research, v. 116, p. 265-283.

Van Achterbergh, E., Ryan, C. G., Jackson, S. E., and Griffin, W. L., 2001, LA-ICP-MS in the Earth Sciences - Appendix 3, data reduction software for LA-ICP-MS, *in* Sylvester, P. J., ed., Short Course volume 29: St.John's, Mineralogical Association of Canada,, p. 239-243.

Wiedenbeck, M., Allé, P., Corfu, F., Griffin, W. L., Meier, M., Oberli, F., Von Quadt, A., Roddick, J. C., and Spiegel, W., 1995, Three natural zircon standards for U-Th-Pb.Lu-Hf, trace element and REE analyses: Geostandards Newsletter, v. 19, p. 1-23.

ELECTRONIC SUPPLEMENT B: THERMAL MODELING

MODEL SCENARIOS

Below we describe three model scenarios that were used to assess the thermal impacts of various geological events. The three scenarios are illustrated in Figure B1.

Scenario 1, time-dependent heating due to a mantle plume

Scenario 1 models the thermal effects of increased temperatures at the base of the lithosphere (LAB = lithosphere–asthenosphere boundary, 120 km depth). This model is intended to test the thermal effects of mantle material coming off the Iceland mantle plume and impinging on the base of the lithosphere in SW Norway. The mantle plume under Iceland is ca. 20 Myr old, which therefore represents the maximum possible duration of this thermal event. The modeled temperature anomalies at the LAB are 100, 200, and 300°C above ambient (1300°C) LAB temperature, and we present the time-dependent thermal evolution at 80 km depth in the lithosphere.

Scenario 2, time-dependent cooling after rift-related heating

Scenario 2 models the thermal decay, or cooling, following a thermal event such as rifting, where additional heat has been supplied to the LAB. The LAB temperature anomalies were set at 100, 200, and 300°C (similar to scenario 1), and run to reach steady-state before the LAB temperature was returned to ambient (1300°C) and allowed to cool for 55 Myr (time since opening of the North Atlantic, the last rift event in the region). We present the time-dependent thermal decay (cooling) at 80 km depth in the lithosphere.

Scenario 3, steady-state thermal anomaly related to radioactively enriched mantle wedge

Scenario 3 models the steady-state thermal anomaly related to a mantle enriched in radioactive elements (U, Th, K). Modeled anomalous heat production rates are 0.1, 0.2, and 0.5 $\mu W/m^3$ above ambient lithospheric mantle heat production of 0.03 $\mu W/m^3$.

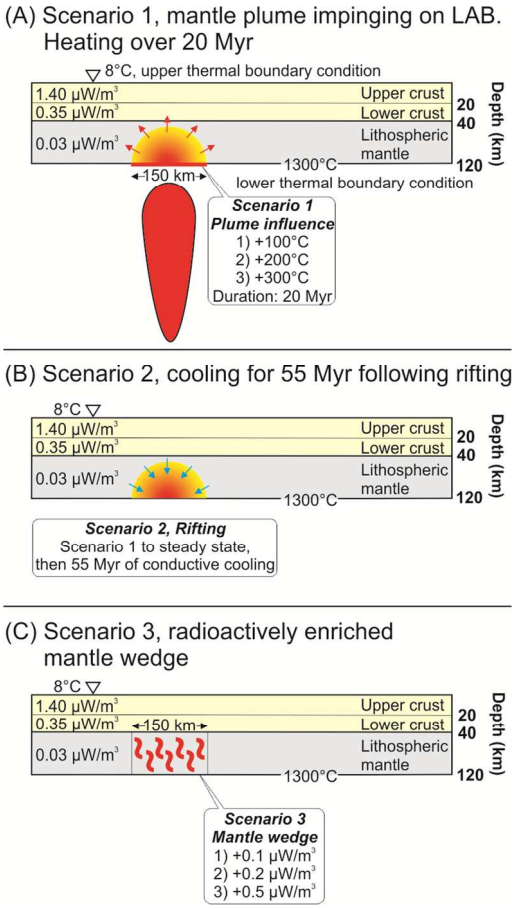

Figure B1. Model scenarios showing model geometry and critical model parameters.

THERMAL PROPERTIES OF ROCKS

The assigned average values of thermal conductivity and specific heat capacity within the lithospheric mantle and crystalline crust are based on published values (Čermak and Rybach, 1982; Clauser, 2011).

The empirical relations (1) and (2) from Vosteen and Schellschmidt (2003) have been taken to calculate the temperature-dependent thermal conductivities for the crystalline crust:

$$k(T) = k_o / (0.99+T(a-b/k_o)) \quad (1)$$

where k(T) is the thermal conductivity of crystalline rocks (W/mK) at temperature T (in K), k_o is the thermal conductivity (W/mK) at 0°C, T is the temperature (in K), a and b are constants: a = 0.0030±0.0015 and b = 0.0042±0.0006.

$$k_o = 0.53k_r +1/2(1.13(k_r)^2-0.42k_r)^{1/2} \quad (2)$$

where k_o is the thermal conductivity of crystalline rocks (W/mK) at 0°C and k_r is the thermal conductivity (W/mK) at room temperature (25°C).

To obtain the temperature- and pressure-dependent thermal conductivities within the lithospheric mantle, the empirical equations (3) and (4) from Hofmeister (1999) have been used:

$$k(T,P) = k_r(298/T)^a \exp(-(4\gamma+1/3)\alpha(T-298))(1+K'_oP/K_o) + k_{rad} \quad (3)$$

$$k_{rad} = 4.7(0.01753-0.00010365T+2.2451T^2/10^7-3.407T^3/10^{11}) \quad (4)$$

where k(T,P) is thermal conductivity (W/mK) at temperature T (in K) and pressure P (in Pa), k_r is the thermal conductivity (W/mK) at room temperature (25°C), T is the temperature (in K), γ is Grueneisen parameter (γ =1 to 1.4), a is the phonon-fitting parameter (a = 0.25 to 0.45), α(T-298) is the volume coefficient of thermal expansion as a function of temperature, K_o is the bulk modulus (K_o=261 GPA), K'_o is the pressure derivative of the bulk modulus (K'_o=5) and k_{rad} is the radiative component of the thermal conductivity, enhanced according to van den Berg et al. (2001).

The radiogenic heat production has been set to 1.4 $\mu W/m^3$ within the upper crystalline crust (0–20 km depth) and 0.35 $\mu W/m^3$ within the lower crystalline crust (20–40 km depth), in agreement with the average values of radiogenic heat production for dominant crustal lithologies

(e.g. Rybach and Čermak, 1982; Slagstad, 2008; Villa et al., 2010). The radiogenic heat production has been taken to be constant (0.03 $\mu W/m^3$) for the entire lithospheric mantle in the case of the scenario with the mantle plume influence (scenarios 1 and 2; Fig. B1) and the reference model for the scenario with a radiogenically anomalous mantle wedge (scenario 3; Fig. B2B). The chosen value of 0.03 $\mu W/m^3$ represents an average radiogenic heat production of the lithospheric mantle beneath cratons (Rudnick and Nyblade, 1999).

METHOD

2D temperature distributions have been modeled using the commercial software package COMSOL Multiphysics. The module "Heat Transfer in Solids" was used to simulate the steady-state and time-dependent heat transfer by heat conduction, which is assumed to be a dominant mechanism of heat transfer at the regional scale within the crystalline crust and the lithospheric mantle. Therefore, these calculations have been performed based on physical principles of the conductive 2D thermal field by solving the heat equation (5):

$$\rho C (\delta T/\delta t) = \nabla \cdot (k \nabla T) + Q \quad (5)$$

where ρ is the density (kg/m^3), C is the heat capacity (J/kgK), T is the temperature (K), k is the thermal conductivity (W/mK), ∇T is the temperature gradient (K/m), t is the time (s), Q is the heat source (radioactive heat production) (W/m^3), δT is the change in temperature per time interval δt, and $\nabla \cdot$ is the operator giving the spatial variation in temperature.

The heat flow q (W/m^2) has been calculated according to Fourier's law of heat conduction (6):

$$q = - k \nabla T \quad (6)$$

where k is the thermal conductivity (W/mK) and ∇T is the temperature gradient (K/m).

MODEL CONFIGURATIONS AND WORKFLOWS

During the 2D thermal calculations, the lateral external boundaries of the models have been assumed to be thermally insulated. A constant temperature of 8°C at the Earth´s surface has been set as the upper thermal boundary condition, whereas the base of the lithosphere (LAB) has been taken as a lower thermal boundary, corresponding to a temperature of 1300°C

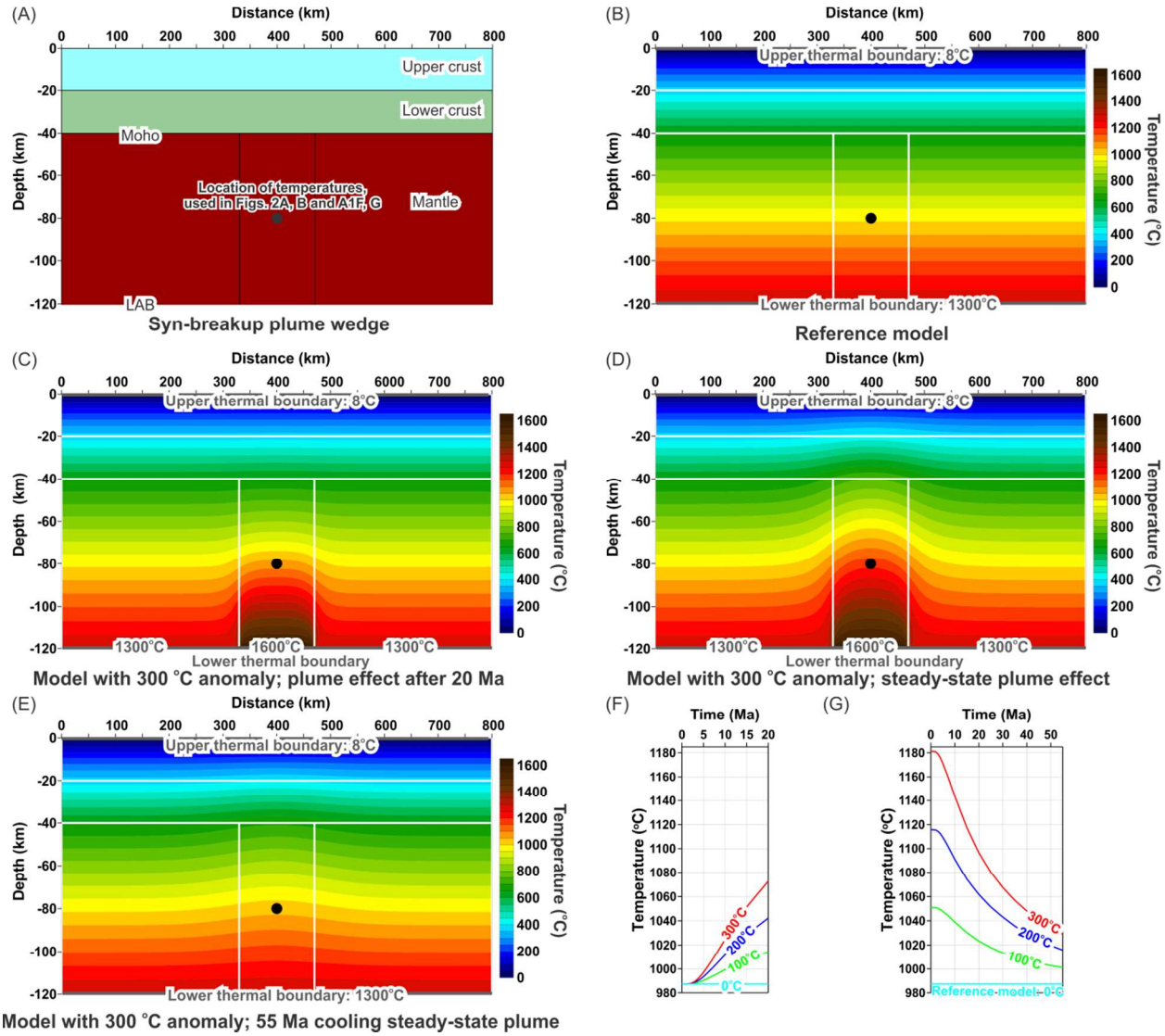

Figure B2. (A) Configuration of the model to estimate the influence of a mantle plume. (B) Reference thermal model (no plume influence). (C) Selected thermal model affected by a mantle plume for 20 Myr with a temperature anomaly of 300°C above ambient LAB temperature. (D) Same as (C), but the model is run until steady state. (E) Temperature distribution after 55 Myr of

cooling from steady-state model in (D). During cooling, the LAB temperature is returned to ambient (1300°C). (F) Temperature evolution over 20 Myr for temperature anomalies of 100, 200, and 300°C above ambient at the LAB. (G) Temperature evolution over 55 Myr during cooling following temperature anomalies of 100, 200, and 300°C above ambient at the LAB that were allowed to reach steady state.

In scenario 1 (mantle plume) and scenario 2 (rifting), the temperature of a 150 km wide portion of the LAB has been increased by 100, 200, and 300°C in three different model runs and allowed to reach steady state, at which point the LAB temperature was returned to ambient (1300°C) and allowed to cool for 55 Myr.

WORKFLOW FOR SCENARIOS 1 AND 2 (MANTLE PLUME AND COOLING AFTER RIFTING)

1. Steady-state thermal calculations for the reference model with 8°C at the top of the model (upper thermal boundary) and 1300°C at the bottom of the model (lower thermal boundary (Fig. B2B).

2. Time-dependent thermal calculations for 20 Myr (Fig. B2C) by setting the LAB temperature over a 150 km wide portion to 1400°C, 1500 °C and 1600 °C. This configuration estimates 100, 200, and 300°C thermal anomalies at the LAB due to a plume impinging at the base of the lithosphere for 20 Myr.

3. The thermal models from point 2 above were then allowed to run until steady-state was reached (Fig. B2D), at which time the temperature over the 150 km wide, anomalous portion of the LAB was returned to ambient (1300°C) and allowed to cool for 55 Myr (Fig. B2E). This model simulates cooling following a long-lived thermal event (rifting in our case) where thermal equilibrium has been reached.

4. Processing the obtained results by producing charts that show how temperatures evolve with time during (scenario 1) and following (scenario 2) external heating (Fig. B2F, G).

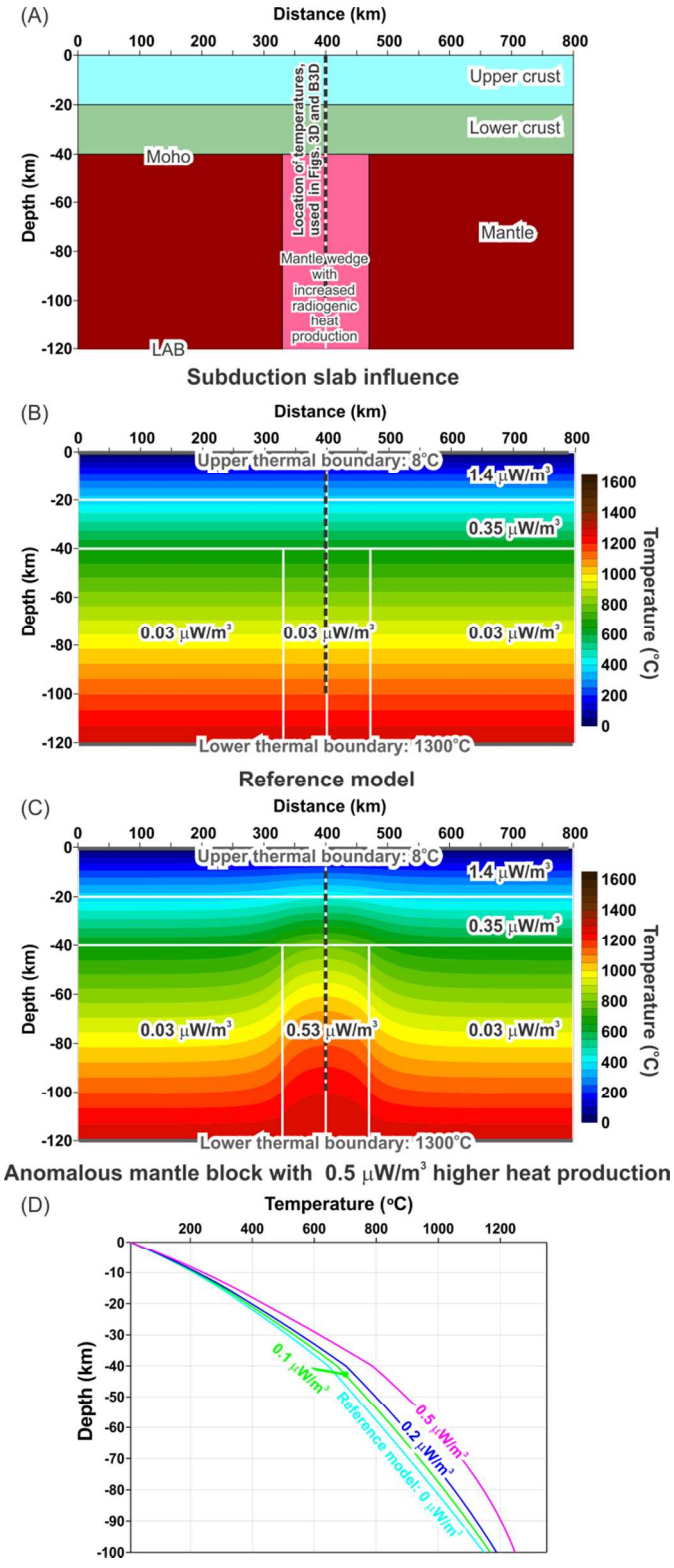

Figure B3. (A) Configuration of the model to estimate the influence of a mantle wedge with increased contents of the radioactive elements. (B) Reference thermal model (no anomalous mantle wedge). (C) Selected thermal model with a radiogenic heat production of 0.5 μW/m^3 within the anomalous mantle wedge. (D) Temperature distribution within the central part of the anomalous mantle wedge for different values of radiogenic heat production.

WORKFLOW FOR SCENARIO 3 (RADIOACTIVELY ANOMALOUS MANTLE WEDGE)

1. Steady-state thermal calculations for the reference model with 8°C at the top of the model (upper thermal boundary) and 1300°C at the bottom of the model (lower thermal boundary (Fig. B3B).

2. Steady-state thermal calculations for anomalous radiogenic heat production rates, 0.1, 0.2, and 0.5 μW/m^3 above ambient lithospheric mantle heat production (0.03 μW/m^3) within the refertilized mantle wedge (Fig. B3C).

5. Processing the obtained results by a chart that shows the temperature anomaly resulting from variable enrichments in heat producing elements in the mantle wedge (Fig. B3D).

REFERENCES

Čermak, V., and Rybach, L., 1982, Thermal properties: Thermal conductivity and specific heat of minerals and rocks, *in* Angenheister, G., ed., Physical Properties of Rocks, Volume Volume 1, subvolume A: Berlin, Springer, p. 305-343.

Clauser, C., 2011, Thermal storage and transport properties of rocks, *in* Gupta, H., ed., Heat capacity and latent heat, Encyclopedia of Solid Earth´s Geophysics, Volume 2: Dordrecht, Springer, p. 1423-1431.

Hofmeister, A. M., 1999, Mantle values of thermal conductivity and the geotherm from phonon lifetimes: Science, v. 283, no. 5408, p. 1699-1706.

Rudnick, R. L., and Nyblade, A. A., 1999, The thickness and heat production of Archean lithosphere; constraints from xenolith thermobarometry and surface heat flow: Special Publication - Geochemical Society, v. 6, p. 3-12.

Rybach, L., and Čermak, V., 1982, Thermal properties: Radioactive heat generation in rocks, *in* Angenheister, G., ed., Physical Properties of Rocks, Volume Volume 1, subvolume A: Berlin, Springer, p. 353-371.

Slagstad, T., 2008, Radiogenic heat production of Archaean to Permian geological provinces in Norway: Norsk Geologisk Tidsskrift = Norwegian Journal of Geology, v. 88, no. 3, p. 149-166.

van den Berg, A. P., Yuen, D. A., and Steinbach, V., 2001, The effects of variable thermal conductivity on mantle heat-transfer: Geophysical Research Letters, v. 28, no. 5, p. 875-878.

Villa, M., Fernandez, M., and Jimenez Munt, I., 2010, Radiogenic heat production variability of some common lithological groups and its significance to lithospheric thermal modeling: Tectonophysics, v. 490, no. 3-4, p. 152-164.

Vosteen, H.-D., and Schellschmidt, R., 2003, Influence of temperature on thermal conductivity, thermal capacity and thermal diffusivity for different types of rock: Physics and Chemistry of the Earth, v. 28, no. 9-11, p. 499-509.